Measurement and modeling of self-broadening coefficients of the $\nu 3$ and $2\nu 3$-$\nu 3$ bands of methyl chloride

N. Dridi, N. Maaroufi, L. Manceron, M. Rotger, H. Aroui

Measurement and Modeling of Self-broadening Coefficients of the ν_3 and $2\nu_3$-ν_3 Bands of Methyl Chloride

N. Dridi , N. Maaroufi , L. Manceron , M. Rotger , H. Aroui

PII: S0022-4073(19)30089-5
DOI: https://doi.org/10.1016/j.jqsrt.2019.06.030
Reference: JQSRT 6551

To appear in: *Journal of Quantitative Spectroscopy & Radiative Transfer*

Received date: 7 February 2019
Revised date: 25 June 2019
Accepted date: 25 June 2019

Please cite this article as: N. Dridi , N. Maaroufi , L. Manceron , M. Rotger , H. Aroui , Measurement and Modeling of Self-broadening Coefficients of the ν_3 and $2\nu_3$-ν_3 Bands of Methyl Chloride, *Journal of Quantitative Spectroscopy & Radiative Transfer* (2019), doi: https://doi.org/10.1016/j.jqsrt.2019.06.030

HIGHLIGHTS

- Self-broadening coefficients have been measured in the ν_3 and $2\nu_3$-ν_3 bands of CH_3Cl.
- The rotational dependencies of broadening coefficients were analyzed.
- The data are modeled using a second-order empirical polynomial.
- Broadening coefficients were predicted using the Robert and Bonamy formalism with parabolic and exact trajectory models.
- The RBE model is not necessary for calculations of self-broadening of CH_3Cl even at low temperature.

Measurement and Modeling of Self-broadening Coefficients of the ν_3 and $2\nu_3$-ν_3 Bands of Methyl Chloride

N. Dridi[1,2], N. Maaroufi[1], L. Manceron[3], M. Rotger[2] and H. Aroui[1*]

[1]*Laboratoire de Spectroscopie et Dynamique Moléculaire, Université de Tunis, Ecole Nationale Supérieure d'Ingénieurs de Tunis, 5 Av Taha Hussein 1008 Tunis, Tunisia.*
[2]*GSMA, UMR CNRS 7331, Université de Reims Champagne Ardenne, Moulin de la Housse B.P. 1039, F-51687 Reims Cedex 2, France*
[3]*Synchrotron Soleil Ligne AILES, BP 48, 91192 Cedex Gif-sur-Yvette, France and MONARIS, UMR 8233 CNRS-UPMC, case 49, 4 place Jussieu, 75252 Cedex Paris, France*

*Corresponding Authors:

Hassen AROUI

Email: haroui@yahoo.fr

Tel. +216 55 560 468, Fax. +216 71391166

Keyword: Methyl chloride, ν_3 and $2\nu_3$-ν_3 bands, Fourier Transform Spectroscopy, Self-broadening coefficients, *J*- and *K*-dependences, exact and parabolic trajectories.

Abstract

High-resolution Fourier Transform spectra have been recorded at room temperature in the frequency region around 13 µm using a high-resolution Fourier transform spectrometer (Bruker IFS 125-HR).

Transitions of both $^{12}CH_3{}^{35}Cl$ and $^{12}CH_3{}^{37}Cl$ isotopologues belonging to the *P*, *Q* and *R* branches of the ν_3 and $2\nu_3$-ν_3 parallel bands have been analyzed to retrieve self-broadening coefficients using a multispectrum fitting procedure that allowed to fit simultaneously the whole set of the experimental spectra recorded at seven pressures of CH_3Cl ranging from 1.02 to 10.24 mbar. Line positions were also derived using a wavenumber calibration performed by the frequencies of OCS transitions.

About 2028 lines with $2 \leq J \leq 59$ and $2 \leq K \leq 13$ have been studied. The rotational *J* and *K* dependencies of the self-broadening coefficients have been clearly observed and modeled using a second-order empirical polynomial. The average accuracy of the line parameters has been estimated to be about 4 and 5 % for the ν_3 and $2\nu_3$-ν_3 bands, respectively.

Using the Robert and Bonamy formalism with parabolic and exact trajectory models, these coefficients were calculated, showing the predominance of the dipole-dipole interaction. The *J* and *K* rotational dependencies are consistent with the measured data. The predicted values confirm that the use of the exact trajectory model does not improve the predicted linewidths for a molecule with a large dipole moment such as CH_3Cl.

1. Introduction

Halogenated hydrocarbon molecules are important species in atmospheric chemistry. A better understanding of this subject could be of highest importance for many environmental problems and warming caused by ozone layer depletion and the greenhouse effect [1].

Among these molecules, methyl chloride is the only chlorinated compound present in the atmosphere with a very predominantly natural origin [2]. This molecule is emitted by the oceans where it is produced by algae [3], forest fires [4] and tropical plants [5]. It is a weekly reactive molecule that can, through the troposphere, reach the stratosphere. Its lifespan in the atmosphere is 1 to 3 years [6].

The release of chlorine radical can then participate in the destruction of ozone through the catalytic of ClO_x cycle [7]. The Montreal Protocol in October 1999 and its subsequent amendments recommended a reduction of the production and the use of CH_3Cl gas as the most abundant halocarbon present in the atmosphere. This molecule represents 30 % of atmospheric chlorine. Otherwise, our knowledge of the global change process in the Earth's atmosphere is primarily based on observations made in situ or by remote-sensing techniques. Measurements performed from the infrared Fourier Transform spectrometer on board the Atmospheric Chemistry Experiment (ACE) satellite allowed to determine the CH_3Cl distribution in both the troposphere and stratosphere [8].

In order to improve the accuracy of atmospheric concentration profile for this molecule, high-resolution spectroscopy is necessary for a regular improvement of atmospheric databases [9,10]. Spectroscopic parameters of methyl chloride have been the subject of numerous experimental and theoretical works in various spectral regions concerning line positions, intensities and broadening coefficients [11-27]. Blanquet *et al.* [11] have measured self-broadening coefficients and line intensities in the ν_3 band of $CH_3{}^{35}Cl$ at low temperature using a tunable diode-laser spectrometer and Voigt profile model. The same group has performed measurements of broadening coefficients and intensities for four overlapped spectral lines of the $^{Q}R(3,K)$ manifold in the same band [12]. The same spectrometer and the same fitting model were used by Bouanich *et al.* [13] to perform measurements of self-broadening of 29 lines (with J up to 50 and K from 2 to 9) of the ^{Q}P- and ^{Q}R-branches in the spectral range 684-767 cm^{-1} of the ν_3 parallel band of $CH_3{}^{35}Cl$. Line broadening parameters were also measured in the ν_5 band by Chackerian *et al.* using a Fourier Transform spectrometer [14]. The authors have also determined rotational constants of the triad formed by the ν_2, ν_5 and $2\nu_3$ bands. Nikitin *et al.* [15-18] have performed numerous experimental and theoretical works about

spectroscopic data of the ground state, and some bands of CH_3Cl lying in a large region of frequency (0–2600 cm^{-1}) using Fourier Transform spectroscopy and an *ab initio* potential energy surface. In Ref. [19], the ν_1, ν_4 and $3\nu_6$ bands of methyl chloride in the 3.4 µm region have been studied to retrieve a large set of line positions and intensities. Guinet *et al.* [20] have performed experimental studies by terahertz techniques and semi-classical calculations of N_2-broadening coefficients of CH_3Cl. Ref. [21] was dedicated to the measurements of line positions, line intensities and self-broadening for several transitions of both $CH_3{}^{35}Cl$ and $CH_3{}^{37}Cl$ isotopologues belonging to the ν_5 band. Self-broadenings of CH_3Cl were measured by Bray *et al.* at room temperature for 527 transitions of the ν_1 band with a high-resolution Fourier spectrometer [22]. In this work, pure rotational lines in the submillimeter-terahertz region were also investigated using two complementary techniques of frequency-multiplication and continuous-wave photomixing. In Ref. [23], the temperature dependence of self- and N_2-broadening coefficients was retrieved using high resolution Fourier transform spectra recorded at temperatures between 200 and 270 K. CH_3Cl-N_2 collisional broadening coefficients of CH_3Cl were measured at room temperature by the same group by means of the same technique [24].

Concerning the theoretical works of methyl chloride, one can cite the works of Refs. [20,22,24-28] where the authors have performed theoretical calculations of self- [22,25,27], N_2-[20,24,26,28] and O_2-[28] broadening coefficients of the methyl chloride at various temperatures. In Refs. [23,25-27], the temperature exponents of linewidths broadenings were derived. In Ref. [27], a semi-empirical method suitable for molecular systems with strong dipole–dipole interactions was used to compute self-broadening coefficients at various temperatures of atmospheric interest. The dependences on the rotational quantum numbers were discussed. References [20,22,24] used the Robert and Bonamy formalism [29] accounting for short-range interactions with an exponential form of the interruption function and the exact trajectory model governed by the Lennard-Jones isotropic potential. Recently, Buldyreva *et al.* [30] performed a review of this formalism using exact trajectory model with an application to the prediction of line broadening and shift coefficients of atmospheric gases.

To our knowledge, the present work reports the first systematic measurements of self-broadening coefficients for 2028 rovibrational transitions in the *P*, *Q*, and *R* branches of ν_3 and $2\nu_3$-ν_3 bands for both $CH_3{}^{35}Cl$ and $CH_3{}^{37}Cl$ isotopologues. These measurements have been performed using Fourier Transform spectra recorded with natural CH_3Cl sample. A

multispectrum fitting procedure was used to fit seven spectra recorded at various pressures of CH_3Cl.

The remainder of this paper is organized as follows. The next sections are devoted to describing the experimental conditions of the recorded spectra as well as the fitting procedures. The derived line positions are presented in Section 4. The results are retrieved and discussed as a function of *J* and *K* quantum numbers in Section 5. The set of measured values of self-broadening coefficients are fitted with an empirical model in Section 6. Semi-classical calculation of line broadening coefficients performed with parabolic and exact trajectories is presented in Section 7. Conclusions are addressed in Section 8. Finally, we propose for the databases a new set of self-broadening coefficients in the 13 µm region corresponding to the ν_3 and $2\nu_3–\nu_3$ bands of CH_3Cl.

2. Experimental conditions

Spectra of pure CH_3Cl in the spectral region from 650 to 800 cm^{-1} have been recorded at the AILES beamline of the SOLEIL Synchrotron facility in Saint-Aubin (France), using a high-resolution Fourier Transform Spectrometer, Bruker IFS 125-HR. This instrument has all the equipment required to operate from the Mid to Far Infrared region. It was equipped with a silicon carbide Globar as a source of the interferometer, a Ge/KBr beam-splitter, a cryogenic filter with a band pass of 500 - 920 cm^{-1}, and an MCT photoconductive detector cooled with liquid Helium down to 4 K [31]. Methyl chloride in natural abundance (74.894 % of $^{12}CH_3{}^{35}Cl$ and 23.949 % of $^{12}CH_3{}^{37}Cl$) was provided by Air Liquide with a stated purity of 99.5 % used without any purification. The spectra were recorded at seven pressures ranging from 1.02 to 10.24 mbar with an MOPD (Maximum Optical Path Difference) of 300 cm which, according to the Bruker definition (R = 0.9/MOPD), corresponds to a resolution of 0.003 cm^{-1}. The detailed experimental conditions are given in Table 1. A background spectrum, recorded with the empty cell, was used as reference in order to limit the baseline variations which may cause errors on the measured linewidths.

The average interferograms were Fourier transformed using the procedure included in the Bruker software OPUS package [32] without apodization, using a Mertz-phase error correction method [33] at 0.5 cm^{-1} phase resolution, and a zero-filling factor of 4. For all recorded spectra, the average signal-to-noise ratios are between 700 and 1500.

The whole optical path was under vacuum, the spectrometer was continuously evacuated below a pressure of 2.3×10^{-4} mbar by a dry pump to minimize the effect on linewidths due to

the atmospheric gases in the optical path. The aperture diameter (1.7 mm) of the spectrometer was set to maximize the intensity of the incident beam on the detector without saturation or loss of spectral resolution. Absorption cell, with a path length of 24.4 ± 0.1 cm and equipped with ZnSe anti-reflective coating windows, was used for all the measurements. The temperature, T = 295 K, of the gas inside the cell was measured using platinum probes on the cell with an accuracy estimated to be ± 1 K. The pressure of the gas was measured using Pfeiffer thermostatic gauge (with a 10.5 mbar full scale) characterized by a stated reading accuracy of 0.2 %. Taking into account the uncertainty arising from small variations of the pressure during the recording, we estimated the measurement uncertainty on the pressure to be about 0.5 %.

Table1: Experimental conditions adapted to the ν_3 and $2\nu_3$-ν_3 bands of CH_3Cl.

Experimental conditions		**Spectrum number and pressures**	
Resolution (cm^{-1})	0.003	Spectrum number	CH_3Cl pressure (mbar)
MOPD (cm)	300	1	1.020 ± 0.002
Optical cell length (cm)	24.4	2	2.100 ± 0.004
Scan number	300-500	3	3.550 ± 0.007
Useful spectral domain (cm^{-1})	650-800	4	5.050 ± 0.010
Beam-splitter	Ge/KBr	5	6.580 ± 0.012
Detector	MCT	6	8.520 ± 0.016
Source	Globar	7	10.240 ± 0.020

The spectrum shown in Fig. 1 is the result of the average of 300 interferometer scans in the region between 650 and 800 cm^{-1} at the pressure of 5.05(1) mbar.

Fig. 2 shows the transmittance spectra of CH_3Cl around 686 cm^{-1} illustrating some lines of the ν_3 band at the pressures of 2.10, 6.58 and 10.24 mbar. The line assignments are taken from HITRAN database [9]. As shown in this figure, the spectra exhibit sinusoidal baseline structure with a separation of 3.5 10^{-3} cm^{-1} between two lobes corresponding to two successive zeros of the sinc function used below to fit the observed spectra. In this figure, one can see that the lines with K = 3p (p integer), have intensity much greater than those with K = 0 and $K \neq$ 3p. This is the case of the $^{Q}P(44,3)$ and $^{Q}P(44,6)$ lines compared to the $^{Q}P(44,4)$ and $^{Q}P(44,5)$ lines with much smaller intensities. Note that the $A_2 \rightarrow A_1$ and $A_1 \rightarrow A_2$ transitions with K = 3p are not resolved, thus the notation A (instead of A_1 or A_2) is used for the symmetry of the levels.

In this figure the close lines, $^{Q}P(44,0,A)$ and $^{Q}P(44,1,E)$, form together a doublet not analyzed in this work, since they can exhibit a non-negligible line mixing effect.

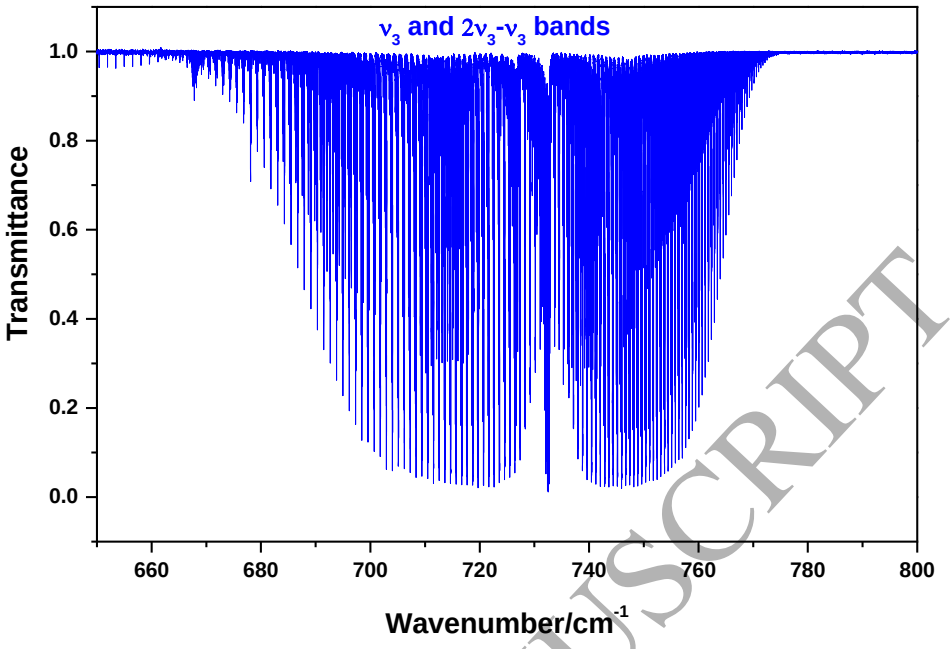

Figure 1: Overview of the high-resolution spectrum of CH_3Cl in the spectral region 650–800 cm^{-1} recorded at a pressure of 5.05(1) mbar. This spectral region corresponds to the absorption of the ν_3 and $2\nu_3$-ν_3 bands.

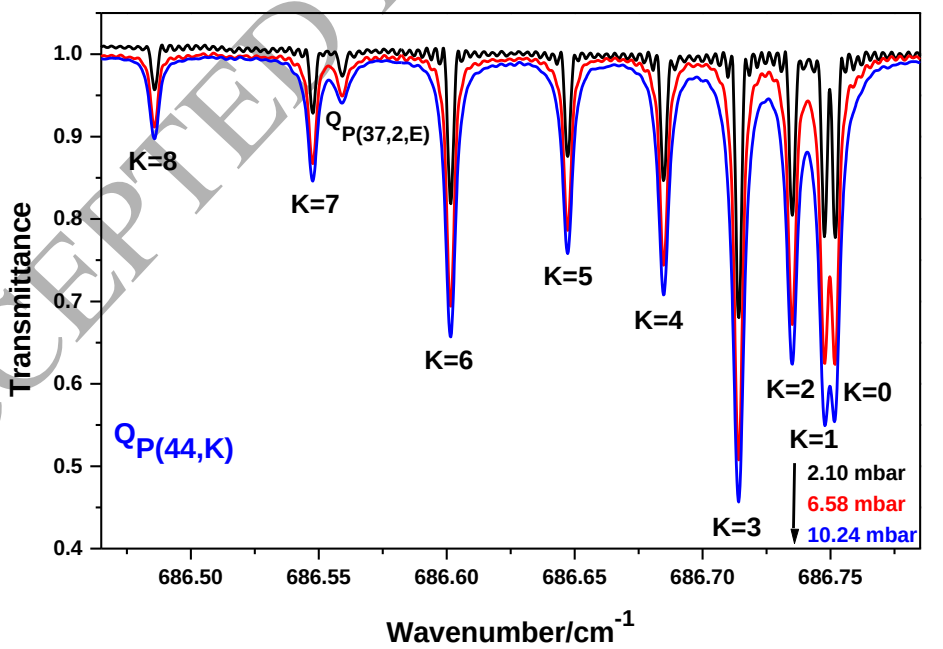

Figure 2: Transmittance spectra of $CH_3{}^{35}Cl$ around 686 cm^{-1} showing some lines of the ν_3 band at pressures of 2.10, 6.58 and 10.24 mbar. The line assignments are taken from HITRAN database [9].

3. Fitting procedures

A multispectrum fitting procedure was used to retrieve the line spectroscopic parameters of the ν_3 and $2\nu_3$-ν_3 bands of CH_3Cl by fitting seven spectra recorded at different pressures. This procedure uses the WSpectra code previously employed in the works of Refs. [34,35]. This code is designed to obtain line spectroscopic parameters with high precision. It is based on a non-linear least squares method in which position, intensity and broadening coefficients were determined by fitting an interval frequency at given pressure. The used code, developed in Brussels [36,37], adjusts a synthetic spectrum to the observed Fourier Transform spectra, using a Levenberg-Marquardt fitting procedure. Due to the low pressures of CH_3Cl considered in this work, the line mixing could be neglected and each line of the synthetic spectra was computed using Voigt profile convoluted with an instrumental line shape function. This function models the contributions of the finite maximum optical path difference of 300 cm and the finite source aperture diameter of the interferometer, fixed here to 1.7 mm. The background in each spectrum was represented by a constant, which was fitted. To compute the Voigt profiles, the Gaussian width was fixed to the value calculated from the Doppler width $\gamma_D \approx 1.32 \times 10^{-3}$ cm^{-1} at T = 295 K.

The fitting procedure requires initial guess values of the line parameters. The line positions and intensities were determined through a peak finding procedure, carried out using the WSpectra program. For each spectrum at a given pressure, the code converged after numerous (≈100) iterations depending on the initial guesses of the adjusted parameters. Note that, in the ν_3 band, doublets formed by rotational components with K = 0 and 1 with the same J but with A or E symmetry, are disregarded since the gap frequency between these components is small enough to induce overlapping and line mixing even at low pressure [38].

An example of the multispectrum fit using the Voigt profile model is presented in Fig. 3 for the $^{Q}P(45,3,A)$, $^{Q}P(45,2,E)$, $^{Q}P(45,1,E)$, and $^{Q}P(45,0,A_2)$ lines of the ν_3 band of CH_3Cl recorded at the pressures of 1.02, 6.58, and 8.52 mbar. The lower panel displays the residual plot of the differences between the observed and calculated spectra. This residual shows no systematic deviation from the Voigt profile. One can try to reduce these residuals by accounting for the Dicke collisional narrowing and speed-dependent effects. As mentioned in some works [38,39], these effects are probably masked by the large self-broadenings of CH_3Cl with a large dipole moment μ = 1.8959 D [40]. These two phenomena could be small enough to be hidden in the noise, then not easily observed with Fourier Transform spectroscopy.

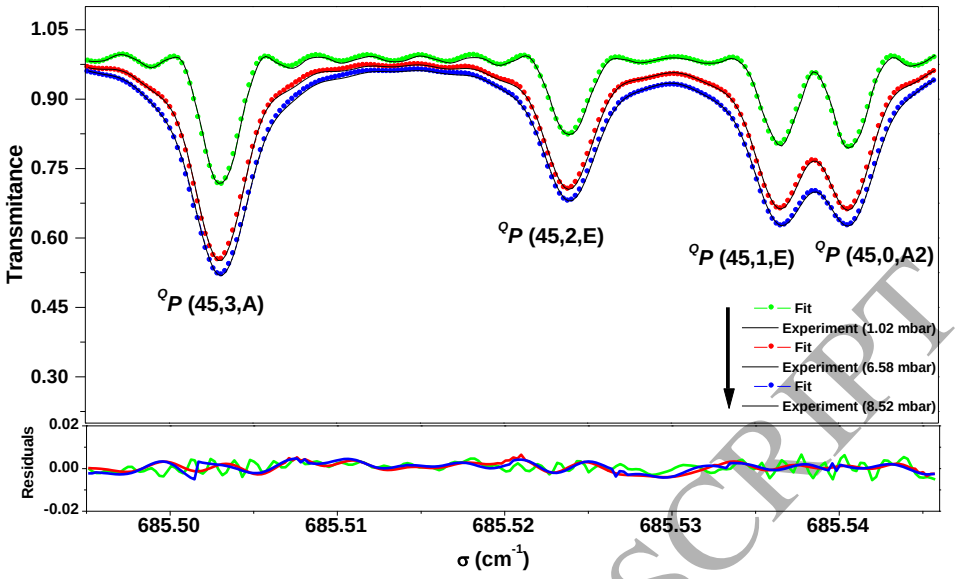

Figure 3 : Fit of the $^{Q}P(45,3,A)$, $^{Q}P(45,2,E)$, $^{Q}P(45,1,E)$, and $^{Q}P(45,0,A)$ lines of the ν_3 band of $CH_3{}^{35}Cl$ recorded at different pressures. The lower panel is a residual plot showing the differences between the observed and calculated spectra.

4. Line positions

To retrieve line positions, we have calibrated the CH_3Cl wavenumbers using OCS transitions of the ν_1 band as etalons. The quantity $\varepsilon = (\sigma_{HITRAN/OCS} - \sigma_{this\ work/OCS})/\sigma_{HITRAN/OCS}$ was computed for around 100 transitions of each spectrum leading to a mean value $< \varepsilon > = (3.9 \pm 0.7) \times 10^{-7}$ which was used to calibrate the seven recorded spectra. This enabled us to determine absolute line positions with a mean accuracy (Standard Deviation) estimated to be 5×10^{-5} cm^{-1}.

Discrepancies between line positions measured in this work and those from the HITRAN [9] database are plotted in Fig. 4. For the two bands, the average difference between our measurements and HITRAN data is equal to 1.35×10^{-4} cm^{-1} (3.2×10^{-5} %) which shows a very good consistency of the present data. The average standard deviation for the ν_3 band is 1.27×10^{-4} cm^{-1} (1.8×10^{-5} %), and that for the $2\nu_3$-ν_3 band is 1.9×10^{-4} cm^{-1} (2.7 10^{-5} %). For most transitions, the differences are very small except for only 63 lines (out of 2028) generally with high J or K values corresponding to weak lines that have a discrepancy greater than 5×10^{-4} cm^{-1}. Finally, note that the ν_3 and $2\nu_3$-ν_3 line positions in the HITRAN database are taken from the analysis of Nikitin *et al*. [15].

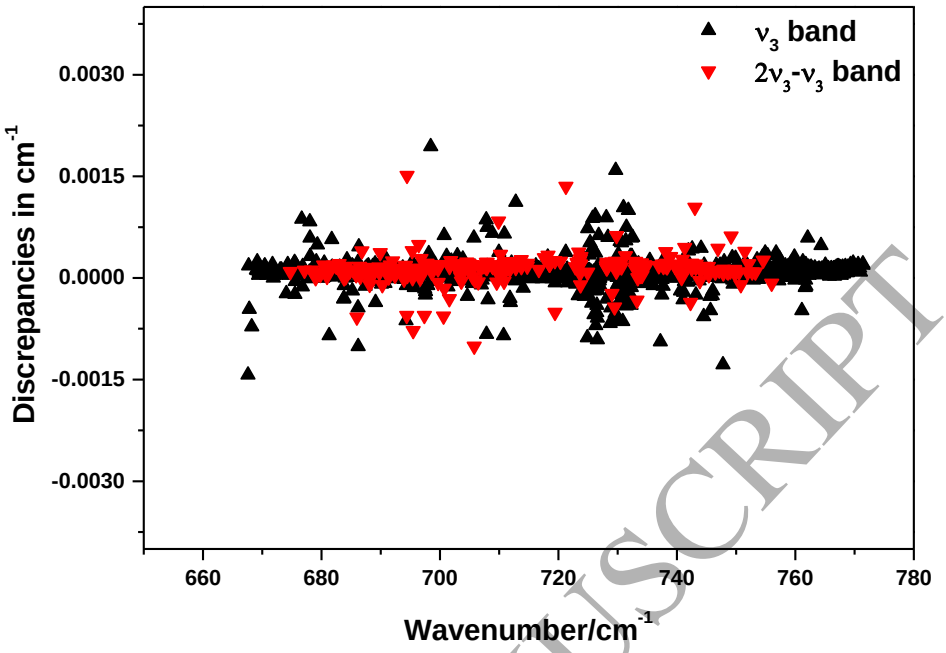

Figure 4: Comparison between line positions of the ν_3 and $2\nu_3$-ν_3 bands measured in this work and those from HITRAN [9].

5. Results, analysis and comparison

In the following, results of self-broadening coefficients are presented and discussed as a function of *J* and *K* rotational quantum numbers and of the branches. These parameters were measured at room temperature *T* = 295 K for 2028 lines pertaining to three branches of each of the ν_3 and $2\nu_3$-ν_3 parallel bands, 1279 and 749 lines for the $CH_3{}^{35}Cl$ and $CH_3{}^{37}Cl$ isotopologues respectively.

5.1 Retrieval of self-broadening coefficients

As expected, the linewidth γ varies linearly with the pressure *P* of CH_3Cl. Thus self-broadening coefficient γ_0 in $cm^{-1}.atm^{-1}$ of a given line was determined as the slope of the straight line deduced from a linear regression passing through the experimental points.

Fig. 5a illustrates a plot of γ versus the pressure *P* of CH_3Cl for the ${}^{Q}P(19,3)$, ${}^{Q}P(19,5)$ and ${}^{Q}P(19,7)$ lines of the ν_3 band. Fig. 5b shows the same plots for the ${}^{Q}P(15,2)$, ${}^{Q}P(20,2)$ and ${}^{Q}P(25,2)$ lines of the $2\nu_3$-ν_3 band. In these figures the error bars were estimated using the following equation accounting for all sources of errors:

$$\frac{\Delta\gamma_0}{\gamma_0} = \left(\left(\frac{SD}{\gamma_0} \right)^2 + \left(\frac{\Delta_{Sys}}{\gamma_0} \right)^2 + \left(\frac{\Delta I}{I} \right)^2 + \left(\frac{\Delta P}{P} \right)^2 + \left(\frac{\Delta L}{L} \right)^2 + \left(\frac{\Delta T}{T} \right)^2 \right)^{1/2}, \quad (1)$$

In this formula, SD is the standard deviation given by the linear fit of the collisional width of each transition as a function of CH_3Cl pressure. $\Delta I/I$ = 0.50 %, $\Delta P/P$ = 0.50 %, $\Delta L/L$ = 0.40 %, and $\Delta T/T$ = 0.34 %, are uncertainties associated with the sample purity, the pressure measurement, the cell length, and the temperature respectively. Δ_{Sys} represents the systematic errors estimated to vary from 1 to 3 % of the broadening coefficients depending essentially on the quality of the fits of the observed lines. Note that the systematic errors and the standard deviation of the fit are the main sources of errors.

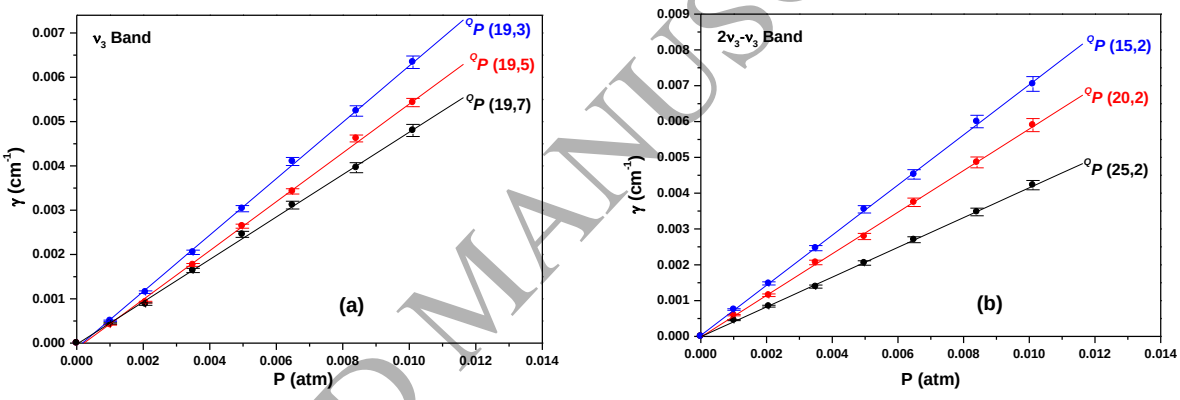

Figure 5: (a) Pressure dependence of the collisional width of the $^{Q}P(J = 19,K)$ for K = 3, 5, and 7 lines of the ν_3 band of $CH_3{}^{35}Cl$. **(b)** Pressure dependence of the collisional width of $^{Q}P(J,K = 2)$ lines for J = 15, 20 and 25 of the $2\nu_3$-ν_3 band of $CH_3{}^{35}Cl$. Error bars are estimated using Eq. (1).

This leads to the accuracy values in Table 2, listing a sample of results of self-broadening coefficients γ_0 for 51 lines of the $^{Q}P(J,2)$ manifold of the ν_3 band. The whole set of the results is given in a supplementary material Table. In these Tables, we have listed for each line the rotational assignment, its transition frequency, its broadening coefficient and its estimated uncertainty. The average values of these uncertainties are 3.9 and 4.9 % for the ν_3 and $2\nu_3$-ν_3 bands respectively. The weak lines are more strongly influenced by baseline uncertainties and results for very weak and/or blended lines with uncertainty greater than 25 % are disregarded.

Table 2: Sample of results of self-broadening coefficients in the $^{Q}P(J,2)$ branch of the ν_3 band of $CH_3{}^{35}Cl$ at 295K.

Iso*	Position		Band	Upper state			Lower state			γ_{exp} ($cm^{-1}.atm^{-1}$)	γ_{Theo} ($cm^{-1}.atm^{-1}$)
241	669.1423022	V3	GROUND	57	2	0E	58	2	0E	0.1112 ± 0.0061	0.1005
241	670.4441960	V3	GROUND	56	2	0E	57	2	0E	0.1189 ± 0.0104	0.1032
241	671.7391072	V3	GROUND	55	2	0E	56	2	0E	0.0848 ± 0.0020	0.1096
241	674.3082188	V3	GROUND	53	2	0E	54	2	0E	0.1031 ± 0.0038	0.1134
241	675.5823260	V3	GROUND	52	2	0E	53	2	0E	0.1360 ± 0.0066	0.1176
241	676.8496232	V3	GROUND	51	2	0E	52	2	0E	0.1412 ± 0.0036	0.1274
241	679.3629949	V3	GROUND	49	2	0E	50	2	0E	0.1550 ± 0.0061	0.1332
241	680.6092383	V3	GROUND	48	2	0E	49	2	0E	0.1399 ± 0.0061	0.1396
241	681.8484643	V3	GROUND	47	2	0E	48	2	0E	0.1330 ± 0.0079	0.1466
241	683.0806528	V3	GROUND	46	2	0E	47	2	0E	0.1668 ± 0.0072	0.1544
241	684.3057028	V3	GROUND	45	2	0E	46	2	0E	0.1647 ± 0.0089	0.1630
241	685.5239461	V3	GROUND	44	2	0E	45	2	0E	0.1573 ± 0.0104	0.1725
241	686.7349917	V3	GROUND	43	2	0E	44	2	0E	0.1819 ± 0.0102	0.1828
241	687.9389840	V3	GROUND	42	2	0E	43	2	0E	0.1848 ± 0.0047	0.1941
241	689.1358750	V3	GROUND	41	2	0E	42	2	0E	0.1784 ± 0.0044	0.2196
241	691.5083652	V3	GROUND	39	2	0E	40	2	0E	0.2315 ± 0.0142	0.2338
241	692.6838744	V3	GROUND	38	2	0E	39	2	0E	0.2203 ± 0.0072	0.2491
241	693.8522940	V3	GROUND	37	2	0E	38	2	0E	0.2620 ± 0.0071	0.2653
241	695.0135639	V3	GROUND	36	2	0E	37	2	0E	0.2888 ± 0.0057	0.2825
241	696.1675887	V3	GROUND	35	2	0E	36	2	0E	0.2571 ± 0.0159	0.3006
241	697.3144685	V3	GROUND	34	2	0E	35	2	0E	0.3040 ± 0.0099	0.3196
241	698.4541897	V3	GROUND	33	2	0E	34	2	0E	0.3118 ± 0.0096	0.3393
241	699.5867184	V3	GROUND	32	2	0E	33	2	0E	0.3904 ± 0.0131	0.3596
241	700.7113540	V3	GROUND	31	2	0E	32	2	0E	0.3805 ± 0.0178	0.3804
241	701.8299047	V3	GROUND	30	2	0E	31	2	0E	0.3471 ± 0.0085	0.4014
241	702.9406581	V3	GROUND	29	2	0E	30	2	0E	0.3521 ± 0.0362	0.4437
241	705.1404273	V3	GROUND	27	2	0E	28	2	0E	0.4672 ± 0.0106	0.4643
241	706.2293478	V3	GROUND	26	2	0E	27	2	0E	0.4673 ± 0.0137	0.4844
241	707.3109589	V3	GROUND	25	2	0E	26	2	0E	0.4817 ± 0.0227	0.5035
241	708.3852601	V3	GROUND	24	2	0E	25	2	0E	0.5143 ± 0.0177	0.5215
241	709.4522349	V3	GROUND	23	2	0E	24	2	0E	0.4953 ± 0.0185	0.5379
241	710.5118695	V3	GROUND	22	2	0E	23	2	0E	0.5620 ± 0.0183	0.5526
241	711.5641165	V3	GROUND	21	2	0E	22	2	0E	0.5519 ± 0.0170	0.5652
241	712.6090072	V3	GROUND	20	2	0E	21	2	0E	0.5950 ± 0.0253	0.5752
241	713.6465110	V3	GROUND	19	2	0E	20	2	0E	0.5480 ± 0.0109	0.5826
241	714.6766273	V3	GROUND	18	2	0E	19	2	0E	0.6217 ± 0.0162	0.5869
241	715.6992948	V3	GROUND	17	2	0E	18	2	0E	0.6155 ± 0.0139	0.5880
241	716.7145205	V3	GROUND	16	2	0E	17	2	0E	0.5862 ± 0.0211	0.5856
241	717.7223180	V3	GROUND	15	2	0E	16	2	0E	0.6111 ± 0.0297	0.5796
241	718.7226719	V3	GROUND	14	2	0E	15	2	0E	0.5627 ± 0.0182	0.5701
241	719.7155511	V3	GROUND	13	2	0E	14	2	0E	0.5708 ± 0.0146	0.5571
241	720.7009270	V3	GROUND	12	2	0E	13	2	0E	0.6159 ± 0.0222	0.5221
241	722.6491638	V3	GROUND	10	2	0E	11	2	0E	0.5183 ± 0.0227	0.5015
241	723.6120006	V3	GROUND	9	2	0E	10	2	0E	0.4783 ± 0.0208	0.4804
241	724.5672843	V3	GROUND	8	2	0E	9	2	0E	0.5175 ± 0.0121	0.4604
241	725.5149877	V3	GROUND	7	2	0E	8	2	0E	0.5160 ± 0.0093	0.4437
241	726.4555115	V3	GROUND	6	2	0E	7	2	0E	0.3825 ± 0.0293	0.4322
241	727.3877467	V3	GROUND	5	2	0E	6	2	0E	0.4245 ± 0.0102	0.4270
241	728.3126969	V3	GROUND	4	2	0^{E}	5	2	0^{E}	0.4451 ± 0.0145	0.4229
241	729.2300757	V3	GROUND	3	2	0E	4	2	0E	0.4193 ± 0.0182	0.3963
241	730.1397758	V3	GROUND	2	2	0E	3	2	0E	0.3464 ± 0.0100	0.1005

*: 24 is the Molecule ID while 1 and 2 refer to isotopologues $CH_3{}^{35}Cl$ and $CH3^{37}Cl$ (HITRAN notations).

5.2 Rotational dependencies of pressure broadening

Extensive measurements of self-broadening coefficients have been obtained for about 2028 lines with $2 \le J \le 59$ and $2 \le K \le 13$ for the ν_3 band, as well as $3 \le J \le 47$ and $0 \le K \le 9$ for the $2\nu_3$-ν_3 band. This large range of measurements allowed rigorous study of the *J*- and *K*-rotational dependencies of the self-broadening coefficients.

For the ν_3 band, these coefficients range from 0.0803 $cm^{-1}.atm^{-1}$ for the $^{Q}P(58,8,E)$ line to 0.6753 $cm^{-1}.atm^{-1}$ for the $^{Q}R(19,3,A)$ line. For the $2\nu_3$-ν_3 band, they vary from 0.1270 $cm^{-1}.atm^{-1}$ for the $^{Q}R(45,3,A)$ to 0.6498 $cm^{-1}.atm^{-1}$ for the $^{Q}R(22,6,A)$ of the $2\nu_3$-ν_3 band. Note that, within the experimental error, no significant discrepancy has been observed between the results of $CH_3{}^{35}Cl$ and $CH_3{}^{37}Cl$. Assuming the effects of the collisions similar for these two isotopologues, one can thus write [22]:

$$\gamma_{0\ Self} = \gamma_{0\ CH_3{}^{35}Cl-CH_3{}^{35}Cl} = \gamma_{0\ CH_3{}^{37}Cl-CH_3{}^{37}Cl} = \gamma_{0\ CH_3{}^{35}Cl-CH_3{}^{37}Cl} = \gamma_{0\ CH_3{}^{37}Cl-CH_3{}^{35}Cl} \qquad (2)$$

Fig. 6 is a plot of the self-broadening coefficients as a function of *J* in the ^{Q}P- and ^{Q}R-branches of $CH_3{}^{35}Cl$ and $CH_3{}^{37}Cl$ with $K = 6$ and $K = 4$ respectively. This figure shows that for a given *K*, the self-broadening coefficients tend to increase until reaching a maximum for $J_{max} \approx 17$, and then started to decrease for higher *J* values. The position of the maximum coefficients is corresponding to the maximum efficiency for collision dominated by the electrostatic interactions. This maximum can be estimated from the resonance condition [41,42]:

$$J_{max} \approx \frac{B_2}{B_1}\frac{\ell_2}{\ell_1} J_{2p} \qquad (3)$$

J_{2p} is the most populated lower level of the perturber: for CH_3Cl at room temperature $J_{2p} = 15$. B_1 and B_2 are the rotational constants of the two partners ($B_1 = B_2$ for self-perturbed CH_3Cl). The spherical harmonic orders ℓ_i depend on the nature of the interaction. For the self-broadening effect, dominated by the dipole-dipole interaction these orders are $\ell_1 = \ell_2 = 1$. Thus the maximum of collision effectiveness is $J_{max} = 15$. As seen by Fig. 6, this value is in reasonable agreement with the experimental observations giving $J_{max} \approx 17$.

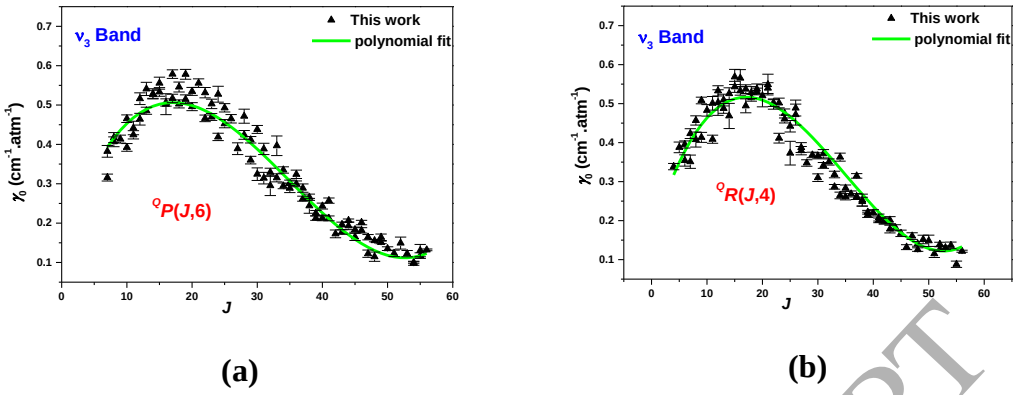

Figure 6: Self-broadening coefficients of the ν_3 band of CH_3Cl versus the rotational quantum number J for $K = 6$ and $K = 4$ for the two branches ^QP and ^QR respectively. Values retrieved from a polynomial fitting of these coefficients are also plotted (see section 6 below).

The same trends are illustrated by Fig. 7 for the broadening coefficients of the $^QR(J,K)$ branch of the $2\nu_3$-ν_3 band for all K manifolds. In these figures, and especially in Fig. 7, the dispersion of the data points is induced essentially by the relatively unresolved or weak lines.

The increase of γ_0 for $J < J_{max}$ could be explained, in part, by the increase of level population with J. While its decrease for $J > J_{max}$ could be explained both by the decreasing of this population with J, and by the increasing with J of the frequency interval between the CH_3Cl levels. Then, collision transfers between these levels could occur with smaller probabilities when J increases. On the other hand, as shown by the supplementary material Table and Fig. 8, the γ_0 values exhibit small decreases with K for a given J. This decrease can be related to the increase of the rotational energy gap with K and the decrease of CH_3Cl rotational population with this quantum number. Plots, not presented here, show the trends of the level population and the level frequency spacing with J and K quantum numbers.

Otherwise, for some molecules, observed or predicted broadening coefficients of lines pertaining to the P, Q and R-branches of the same K and m (m = -J, J and J+1 for the P, Q and R branches respectively) can be compared. At first sight, the supplementary material Table exhibits a small branch effect but without any systematic trends. The mean value of differences in percent between the transitions, with same K and m, of the R and P branches of the ν_3 band does not exceed 7 %. About two third (325 out of 478) of the lines have values of difference smaller than 5 %, thus showing no branch effect.

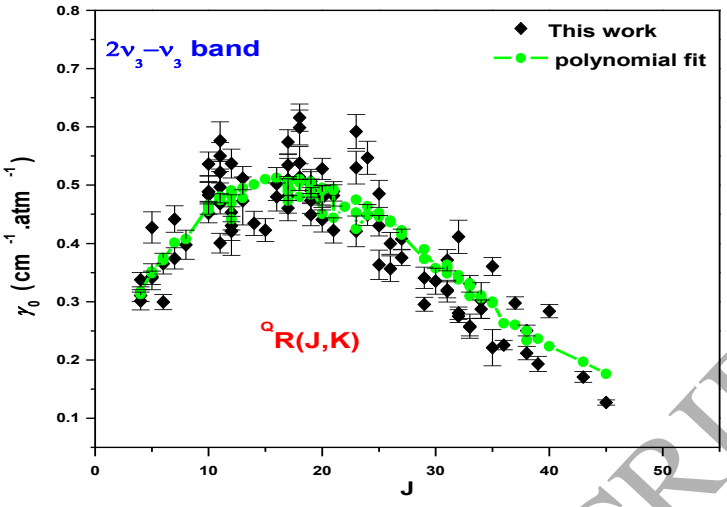

Figure 7: Self-broadening coefficients of CH_3Cl versus the rotational quantum number *J* for all *K* values of the $^{Q}R(J,K)$ branch of the $2\nu_3$-ν_3 band. Values retrieved from calculations using the polynomial fitting of these coefficients are also plotted (see below).

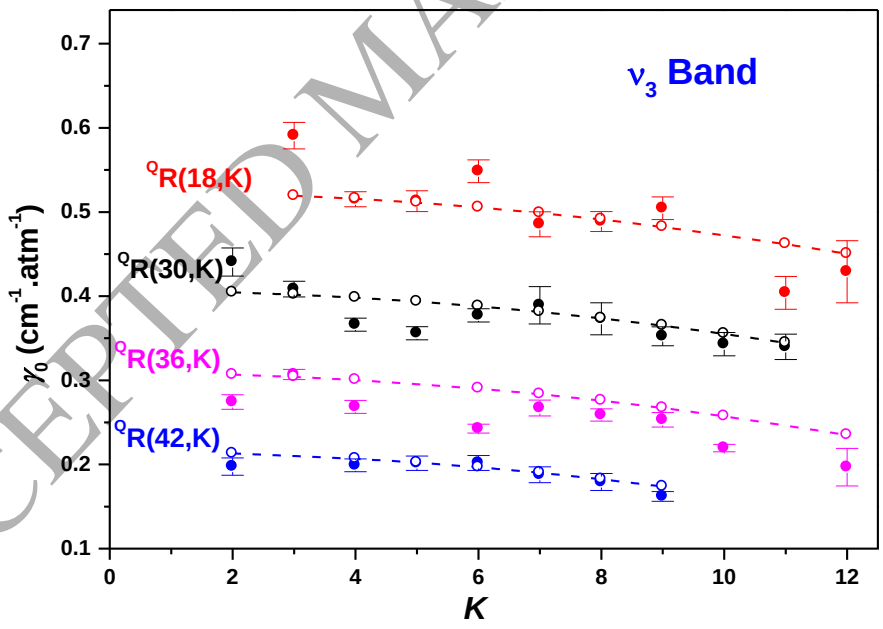

Figure 8: Plots of self-broadening coefficients of the ν_3 band displayed versus rotational quantum number *K* for *J* = 18, 30, 36, and 42. The Solid circles represent the measured broadening coefficients from this work and the dashed lines plus open symbols present the values retrieved from calculations using the polynomial fitting of these coefficients (see section 6 below).

Fig. 9 shows the plot of measured self-broadening coefficients versus the quantum number *m*. The curves are symmetric with respect to the origin, showing no variation of the broadening coefficients with the type of branch.

For the ^{Q}Q branch the number of measured lines is very small compared to that of ^{Q}P and ^{Q}R branches. As observed in this figure, the small difference between the ^{Q}Q sub-branch and the other two sub-branches could be attributed to line mixing which is generally more pronounced in *Q* branches. Because of this small number of studied lines, we cannot confirm this interpretation with high confidence.

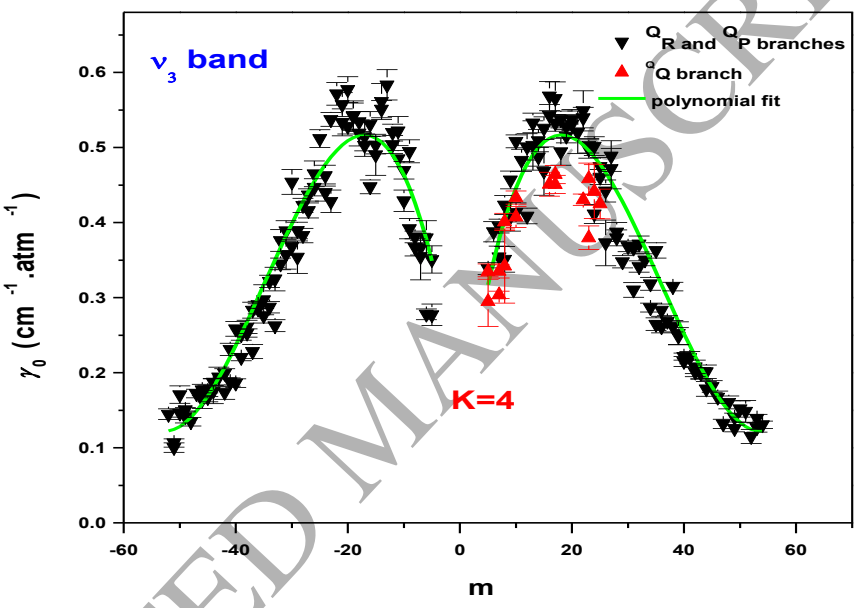

Figure 9: Self-broadening coefficients of CH_3Cl versus the rotational quantum number *m* for *K* = 4 for the sub-branches $^{Q}P(J,K=4)$, $^{Q}R(J,K=4)$ and $^{Q}Q(J,K=4)$ of the ν_3 band. Those from the polynomial fitting are also displayed (see section 6 below).

5.3 Comparison with previous measurements

Many authors have discussed the vibrational effect on the pressure broadening process. In most cases the comparison of the results of different bands exhibits small vibrational dependence. This dependence can arise from the variation of the intermolecular potential with the vibrational mode implying the changes of the rovibrational wave-function, energy gaps and from the transition collisional probability with vibrational excitations.

The present results of self-broadening coefficients can be compared with the results of Refs. [9,13,21,22]. The present work reproduces the systematic *J* and *K* quantum numbers

dependencies observed in these references, namely, an increase with *J*, followed by a maximum then a decrease. The comparison with [9, 13, 22] is illustrated by Fig. 10 plotting the variation of γ_0 versus *J* for the $^{Q}P(J,K{=}5)$ manifold of the ν_3 band and those from the above references for parallel bands and for the same manifolds. Note that the broadening coefficients of HITRAN database [9] are from computation using the semi-empirical prediction of Ref. [27].

The mean values of the differences between the present results and those of Ref. [9] are about 8 % and 10 % for the ν_3 and $2\nu_3$-ν_3 bands respectively. For the ν_3 band the difference becomes about 7 % when the comparison is performed with the measured values of Ref. [13]. Within the uncertainties of various measurements (which are around 5 % for each band), our results of the ν_3 band are in satisfactory agreement with the data of these references. Despite a relatively larger difference for the $2\nu_3$-ν_3 band (10 %), we can conclude an overall agreement with the data of Ref. [9] since this band exhibits weak line intensities compared to that of ν_3 band.

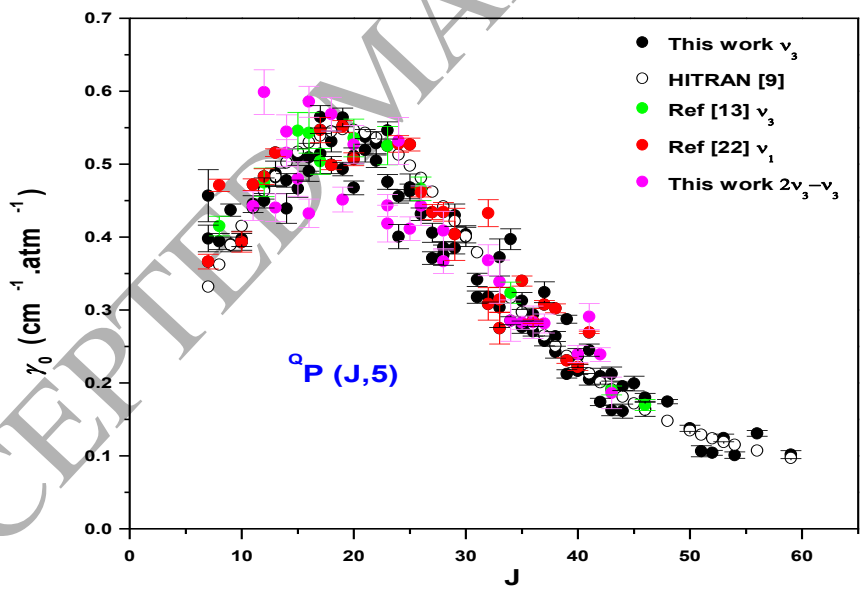

Figure 10: Comparison of the present data of self-broadening coefficients of CH_3Cl in the ν_3 band with those of $2\nu_3$-ν_3 band and of Refs. [9,13,22]. The data are plotted as a function of the rotational quantum number *J* for *K* = 5 in the sub-branch $^{Q}P(J,5)$.

Let's see if we can detect a vibrational effect on the pressure broadening phenomena. The values of the ν_3 band are relatively greater than those of the $2\nu_3$-ν_3 band with a mean value of

difference of about 13 % exhibiting a quite small vibrational effect. Indeed, for 162 lines studied in common in the two bands, 125 lines of ν_3 have γ_0 values greater than that of the $2\nu_3$-ν_3 band.

On the other hand, the absolute values of the differences between the present results for the ν_3 band and those for ν_1 [22] and for ν_5 [21] are about 7 % and 8 %, respectively. Since the signs of these differences are not systematic, and are within the experimental uncertainties of the measured data sets, we cannot clearly judge about this effect.

6. Polynomial fit of self-broadening coefficients

In order to fit the rotational dependence of pressure broadening and to provide empirical interpolation and extrapolation models for all rovibrational lines of a given band, some authors used empirical polynomial equations. For halogenated hydrocarbon molecules, Refs. [22,43,44] proposed an empirical power law to fit the J and K dependencies of their pressure broadening linewidths. Nevertheless, some polynomial formulas fail to fit the observed broadening coefficients of lines with low or high values of J and K. Other fits were satisfactory for nonpolar buffer gases, but fit poorly the self-broadening at low J quantum number. The measured broadening coefficients of the six branches of the ν_3 and $2\nu_3$-ν_3 bands considered in this work were fitted using the following equation:

$$\gamma_0(J,K) = A_0 + A_1 J + A_2 J^2 + A_3 K^2 + A_4 J^3 \qquad (4)$$

The parameters A_0, A_1, A_2, A_3 and A_4 are in unit of $cm^{-1}.atm^{-1}$. These parameters were determined using a nonlinear least-square method that adjusts this equation to the experimental values of broadening coefficients listed in the supplementary material Table. The fits were performed simultaneously for all lines of each band, namely 1762 and 266 data points for the ν_3 and $2\nu_3$-ν_3 bands, respectively.

The parameters derived from these fits are given in Table 3 along with their uncertainties estimated as the fit standard deviations. These uncertainties do not explicitly reveal the errors from the physical parameters intervening in the experiment, but implicitly reflect the accuracy of linewidth measurements. As it can be seen by this Table, all parameters are well determined. For the two bands, the two sets of parameters have the same signs. This is expected, since the two bands have the same variation according to J and K. The A_2 and A_3 values are negative and all the other parameters are positive. For the two bands, the A_3 values

corresponding to the quadratic K-dependence of γ_0, are large ($\approx 10^{-3}$) compared to the A_4 values, with a negative sign for the two bands and accuracies of about 6 % and 20 % for the ν_3 and $2\nu_3$-ν_3 bands, respectively. The values of A_3 are in the same order of magnitude than the values of the A_2 parameter expressing the J-quadratic dependence. These two parameters demonstrate the strong variation of γ_0 with J^2 and K^2, as observed previously in Refs. [21, 22, 43, 44] where the measured values of broadening coefficients exhibit a clear linear trend with K^2. The A_4 values of the two bands are positive and about two orders of magnitude smaller than the values of A_3 showing a small variation of linewidth with J^3.

Using the values of the parameters listed in this Table and Eq. (4), we have calculated the broadening coefficients of the studied lines of the supplementary material Table. We reproduce the rotational dependencies of the experimental line broadening with an average difference of about 9 % and 10 % for the ν_3 and $2\nu_3$-ν_3 bands, respectively. However, for some branches of the two bands, the lines with high or low J values have less success to be fitted by Eq. (4) and the parameters of Table 3. Figs. 6, 7, 8 and 9 show the comparison between the values retrieved by the polynomial fit and the measured values of some sub-branches of the two bands, illustrating an excellent agreement between the two sets of values.

Table 3: Best-fit coefficients A_i in $cm^{-1}.atm^{-1}$ of Eq. (4) used to reproduce the measured self-broadening coefficients of the ν_3 and the $2\nu_3$-ν_3 bands.

Parameters	ν_3 band	$2\nu_3$-ν_3 band
A_0	0.1645 ± 0.0079	0.1508 ± 0.0229
A_1	0.0473 ± 0.0010	0.0497 ± 0.0037
$A_2\times10^3$	-1.833 ± 0.038	-2.030 ± 0.175
$A_3\times10^3$	-0.511 ± 0.032	-0.615 ± 0.102
$A_4\times10^5$	1.752 ± 0.041	2.089 ± 0.245

7. Theoretical calculations

7.1 Introduction

Semi-classical calculations accounting for the short-range intermolecular interactions employ traditionally parabolic trajectory curved by the isotropic part of the interaction potential [29]. In these calculations, the second order interruption function is written as a function of the distance of the closest approach, r_c. However, for many collisional systems, the use of the exact trajectory model can lead to an improvement of theoretical linewidths [45-48], at the cost of CPU time for the numerical integration of the interaction potential along the

trajectories. Among these references only the reference [48] uses the bi-resonance functions of Starikov [49]. At room temperature the two trajectory models (noted in the following RBP and RBE for the parabolic and exact trajectories respectively) lead to very close values of broadening coefficients.

At low temperature, the usual hypothesis of the RBP model is supposed to progressively lose its validity, and the RBE approach should derive more efficient predictions to reproduce the measured linewidths [46]. The present results will thus be used as a comparative test of the model performance, in the limit case of a strongly polar symmetric top molecule.

7.2 Computations of pressure broadening coefficients

In order to insure the most precise prediction of CH_3Cl self-broadening coefficients, for the studied collisional system, we perform computations of these coefficients with the RBP and RBE models. Both models assume that the trajectory is governed by the isotropic part of the intermolecular potential in the Robert and Bonamy framework [29].

Within this framework, the pressure broadening half-width of an optical transition i →f is given by:

$$\gamma = \frac{n_p}{2\pi c}\sum_{J_2K_2}\rho_{J_2K_2}\int_0^\infty vF(v)dv\int_{r_{c0}}^\infty 2\pi r_c\left(\frac{v_c'}{v}\right)^2\left\{1-\exp\left[-\left(\Re eS_{2,i}^{outer}+\Re eS_{2,f}^{outer}+\Re eS_2^{middle}\right)\right]\right\}dr_c\,, \qquad (5)$$

where n_p is the number density of perturbing molecules, $\rho_{J_2K_2}$ is the relative population of the rotational level of the ground vibrational state of the perturber, v is the relative velocity between the absorber and the perturber, $F(v)$ is the Maxwell velocity distribution, v_c' is the equivalent straight trajectory velocity and r_{c_0} is the value of the position r_c for the distance of the closest approach. $S_{2,i}^{outer}$, $S_{2,f}^{outer}$ and S_2^{middle} are the second-order terms of the interruption function derived from the anisotropic part of the potential [29,50].

Since the electrostatic interactions dominate the broadening of CH_3Cl with a large dipole moment, μ = 1.8959 D [40], this potential can be written as:

$$V_{aniso} = V_{\mu_1\mu_2} + V_{\mu_1Q_2} + V_{Q_1\mu_2} + V_{Q_1Q_2} \qquad (6)$$

The subscripts 1 and 2 refer to the absorbing and the perturbing molecules, and Q is the quadrupole moment of CH_3Cl. In the computation, we have considered the $\Delta K = 0$ transitions

induced by collision, associated with the selection rules ΔJ = 0, ± 1 for the dipolar transitions and ΔJ = 0, ± 1, ± 2 for the quadrupolar transitions. We used the RBP and RBE trajectory models both calculated using the 12-6 Lennard-Jones potential.

Self-broadening coefficients γ_0 in $cm^{-1}.atm^{-1}$ were computed for two temperatures T = 295 and 200 K. The intermolecular distance of closest approach r_{c0} was computed to be 3.47 and 3.50 Å for T = 295 and 200 K, respectively. However, because of the strong electrostatic interactions, the calculations overestimate the measured values. Thus, the upper limit of r_c was set to r_{cmax} = 25 Å. It is the appropriate value of r_{cmax} that allowed us to achieve results in good agreement with the measured values.

The computation included the rotational states of the perturber in the ground state with K_2 values varying from 0 to 17, that are weighted by the Boltzmann and nuclear spin factors. The values of the rotational partition function Q_{rot} are taken from Ref. [25]: Q_{rot}(T=200K) = 1916.32, Q_{rot}(T=296 K) = 3447.68.

The rotational constants used in the computations are given in Table 4. The quadrupole moment Q, and the Lennard-Jones parameters σ and ε of CH_3Cl are, respectively, Q = 1.23 DÅ [51], σ = 3.584 Å [28] and (ε) = 368.4 K [28].

Table 4. Molecular parameters used in the computation of self-broadening coefficients of CH_3Cl [16].

A_0 (cm^{-1})	B_0 (cm^{-1})	D_J (10^{-7} cm^{-1})	D_{JK} (10^{-6} cm^{-1})	D_K (10^{-5} cm^{-1})
5.2053361	0.44340278	6.0381	6.358	8.2965

7.3 Results and discussions

The calculations were performed for the experimental transitions of the ν_3 band for $CH_3{}^{35}Cl$ isotopologue and are compared to the experimental values in Table 2 and in Fig. 11. We reproduce the rotational J- and K-dependencies of the measured values of the ν_3 band. Note that the contribution to the values of broadening coefficients derived from the strong dipole-dipole interaction is about 95 % of that retrieved from the total electrostatic interactions.

At room temperature (T = 295 K), within the various uncertainties both in the experiments and in the calculations, the agreement between measured and predicted values using RBP and RBE models is satisfactory. Indeed, for almost all lines of the ν_3 band, the differences in

percent between measured and calculated values of self-broadening coefficients do not exceed 21 %, with a mean value of 7 %.

In Ref. [22] the authors used the same method with exact trajectory model; the comparison with these values gives a difference of 4.6 %. This difference shows that our results are in good agreement with this reference. We have also computed the broadening coefficient using the Anderson-theory formalism with a straight-line trajectory. The results are in satisfactory agreement with those obtained with parabolic and exact trajectory with a mean difference of about 4.3 %.

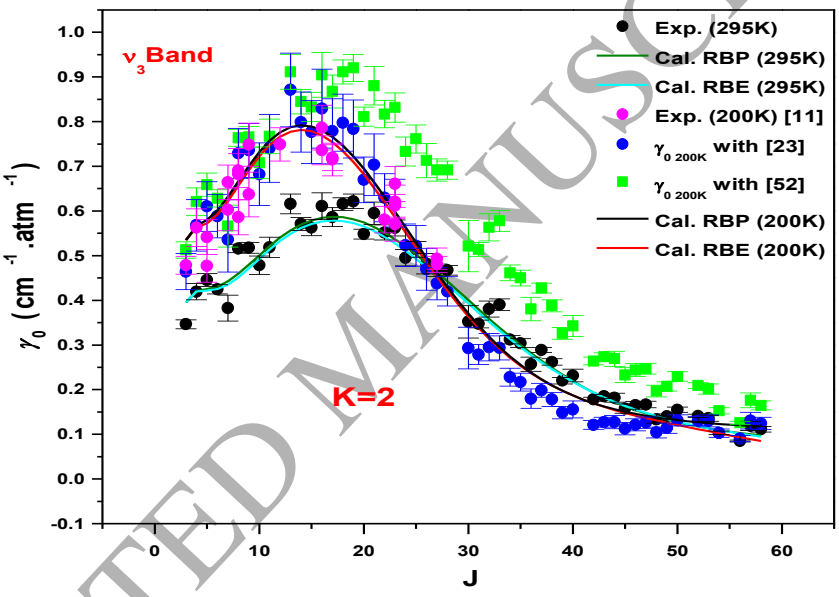

Figure 11 : Computed values of broadening coefficients for the $^{Q}P(J,2)$ sub-branch of the ν_3 band using the RBP and RBE trajectory models compared to the measured data at two temperatures T = 200 and 295 K. ■ and • are values deduced from those at room temperature using Refs. [52] and [23] respectively. The measured data at T = 200K of Ref. [11] are also plotted for comparison.

Fig. 11 compares the predicted values by the RBP and the RBE models with the experimental values of the ν_3 band at 200 and 295 K. Those at 200 K have been determined by scaling our measured values at T = 295 K by the well-known empirical power law:

$$\gamma_0(T) = \gamma_0(T_0)\left(\frac{T_0}{T}\right)^{\alpha} \qquad (7)$$

In this equation, $\gamma_0(T_0)$ is the broadening coefficient at the reference temperature T_0 = 200 K and α is the temperature exponent.

Two methods were used to determine $\gamma_0(T$=200 K). As a first stage, we have estimated the value of α from the usual expression, $\alpha = \frac{n+1}{2(n-1)}$ given by Birnbaum [52]. For the dominant dipole–dipole interaction, such as CH_3Cl-CH_3Cl, with the exponent of the intermolecular potential n = 3, we obtain α = 1 for all lines of a given molecule. The retrieved values of $\gamma_0(T$=200K) using Eq. (7) are plotted with green color in Fig. 11 illustrating a quite equidistant separation from the curve plotting $\gamma_0(T$=295K) for J > J_{max} with greater values for T = 200 K.

In a second step, the temperature exponents are taken from the second order J-polynomial equation of the precise work of Ref. [23], which illustrates a rotational dependence of this exponent. Although independent of the K quantum number, this polynomial equation permits to calculate a broadening coefficients exhibiting the same J-evolution than that of Fig. 1 of Ref. [23]. When this dependence is plotted in Fig. 11 a curve crossing at about J = 25 is occurring, leading for $J \geq 25$ to values of $\gamma_0(T$=200K) smaller than $\gamma_0(T$=295 K) reversing the sign of temperature exponents and validating its negative sign. This sign reversal is rarely observed experimentally, but usually predicted by theoretical calculations [25-27].

When comparing the values at 200 K, determined using the relation in Ref. [52], with the measured values of Blanquet *et al.* [11] measured for J ≤ 27, the difference is about 15%. This difference is greatly reduced to 6.5 % when the comparison is performed with the values determined using the method of Ref. [23]. As shown by Fig. 11, the values of $\gamma_0(T$=200 K) retrieved from the computation with either the RBP or RBE trajectory models is quite different (about 28 %) from the values deduced using the Birnbaum formula [52], inciting research communities to perform measurements of pressure broadening and pressure shifting parameters as a function of temperature aiming determination of reliable values of temperature exponents.

Comparing the predictions made using the RBP and RBE trajectory models with the $\gamma_0(T$=200 K) values determined using the data of Ref.[23], a much better agreement is found. The differences are 8 and 7 % for T = 200 and 295 K, respectively with either RBE or RBP models. Nearly the same precision is achieved with the two trajectory models. The differences between the two predictions are 4 % and 2 % for T = 200 and 295 K, respectively.

As a consequence, these calculations predict more precisely the measured values of the CH_3Cl self-perturbed as stated by Ref.[30] for collisions with strong electrostatic interaction.

8. Conclusion

Using high-resolution Fourier Transform spectra at room temperature and a multispectrum fitting technique, line positions and self-broadening coefficients have been retrieved for about 2028 transitions belonging to the ν_3 and $2\nu_3$-ν_3 bands of methyl chloride in the 13 µm region. The accuracy has been estimated to be about 4-5 %, depending on the transitions. The *J*- and *K*-rotational dependencies of self-broadening coefficients have been analyzed and modeled showing a good consistency with previous measurements of the literature, with no evidence of systematic differences between the vibrational bands or between the two isotopologues. For all lines and pressures considered in this work, the Voigt absorption profile is adequate to fit the observed line profiles.

Calculations were carried out using two trajectory models at 200 K and 295 K temperatures showed an excellent consistency with the experimental data, indicating that the use of the RBE model for the prediction of measured broadening coefficients is not necessary in the case of CH_3Cl self-perturbed. The RBP model and even the straight-line trajectory can provide reliable prediction for the long range strong interactions considered in the present work.

Finally, since the large discrepancy between the broadening coefficients deduced from the exponent coefficient of Birnbaum [52] and those from precise measurements of Ref. [23], we invite research communities to perform measurements of pressure broadening and pressure shifting parameters as a function of temperature for reliable determination of temperature exponents.

Acknowledgments

The authors are grateful to Dr. J. Auwera (**Université Libre de Bruxelles)** for making available his fitting program and for constructive discussions.

References

[1] Solomon S, Garcia RR, Rowland FS, Wuebbles DJ. On the depletion of Antarctic ozone, Nature 1986;321:755-8.

[2] World Meteorological Organization, Scientific Assessment of Ozone Depletion: 2002. Report 2002.

[3] Khalil MAK, Rasmussen RA. Atmospheric methyl chloride. Atmos. Environ 1999;33:1305-21.

[4] Lobert JM, Keene WC, Logan JA, Yevich R. Global chlorine emissions from biomass burning: Reactive Chlorine Emissions Inventory. JGR Atmospheres 1999;104:8373-89.

[5] Yokouchi Y, Noijiri Y, Barrie LA, Toom-Sauntry D, Machida T, Inuzuka Y, Akimoto H, Li HJ, Fujinuma Y, Aoki S. A strong source of methyl chloride to the atmosphere from tropical coastal land. Nature 2000;403:295-8.

[6] Yasuko Y. Global sources and distribution of atmospheric methyl chloride. PhD Thesis, Georgia Institute of Technology, 2006.

[7] Molina MJ, Rowland FS. Stratospheric sink for chlorofluoromethanes: chlorine atom-catalysed destruction of ozone. Nature 1974;249:810-12.

[8] Kaley AW, Weigum N, McElcheran C, Taylor JR. Global methyl chloride measurements from the ACE-FTS instrument. International Symposium on Molecular Spectroscopy Department of Chemistry The Ohio State University, TI-09: 2009.

[9] Gordon IE, Rothman LS, Hill C, Kochanov RV, Tan Y, Bernath PF *et al*. The HITRAN 2016 molecular spectroscopic database. J Quant Spectrosc Radiat Transfer 2017;203:3-69.

[10] Jacquinet-Husson N, Armante R, Scott NA, Chedin A, Crepeau L, Boutammine C, Bouhdaoui A *et al*. The 2015 edition of the GEISA spectroscopic database. J Mol Spectrosc 2016;327:31-72.

[11] Blanquet G, Warland J, Populaire JC, Bouanich JP. Self-broadening coefficients and line strengths in the ν_3 band of $CH_3{}^{35}Cl$ at low temperature. J Quant Spectrosc Radiat Transfer 1995;53:211-19.

[12] Blanquet Gh, Coupe P, Walrand J, Bouanich JP. Determination of broadening coefficients and intensities for overlapping spectral lines with application to the ${}^{Q}R(3,K)$ lines in the ν_3 band of $CH_3{}^{35}Cl$. J Quant Spectrosc Radiat Transfer 1994;51:671-8.

[13] Bouanich JP, Blanquet Gh, Walrand J. Diode-laser measurements of self-broadening coefficients and line strengths in the ν_3 band of $CH_3{}^{35}Cl$. J Quant Spectrosc Radiat Transfer 1994; 51:573-8.

[14] Chackerian C, Brown LR, Lacome N, Tarrago G. Methyl chloride ν_5 region lineshape parameters and rotational constants for the ν_2, ν_5 and $2\nu_3$ vibrational bands. J Mol Spectrosc 1998;191:148-57.

[15] Nikitin AV, Féjard L, Champion JP, Bürger H, Litz M, Colmont JM, Bakri B. New measurements and global analysis of chloromethane in the region from 0 to 1800 cm^{-1}. J Mol Spectrosc 2003;221:199-212.

[16] Nikitin AV, Champion JP. New ground state constants of $^{12}CH_3{}^{35}Cl$ and $^{12}CH_3{}^{37}Cl$ from global polyad analysis. J Mol Spectrosc 2005;230:168-73.

[17] Nikitin AV, Champion JP, Bürger H. Global analysis of $^{12}CH_3{}^{35}Cl$ and $^{12}CH_3{}^{37}Cl$: simultaneous fit of the lower five polyads (0-2600 cm^{-1}). J Mol Spectrosc 2005;230:174-84.

[18] Nikitin A. Vibrational energy levels of methyl chloride calculated from full dimensional ab initio potential energy surface. J Mol Spectrosc 2008;252:17-21.

[19] Bray C, Perrin A, Jacquemart D, Lacome N. The ν_1, ν_4 and $3\nu_6$ bands of methyl chloride in the 3.4 µm region: Line positions and intensities. J Quant Spectrosc Radiat Transfer 2011;112:2446-62.

[20] Guinet M, Rohart F, Buldyreva J, Gupta V, Eliet S, Motiyenko R, Margulès L, Cuisset A, Hindle F, Mouret G. Experimental studies by complementary terahertz techniques and semi-classical calculations of N_2-broadening coefficients of CH_3Cl. J Quant Spectrosc Radiat Transfer 2012;113:1113-26.

[21] Barbouchi Ramchani A, Jacquemart D, Dhib M, Aroui H. Line positions, intensities and self-broadening coefficients for the ν_5 band of methyl chloride. J Quant Spectrosc Radiat Transfer 2013; 120:1-15.

[22] Bray C, Jacquemart D, Lacome N, Guinet M, Cuisset A, Eliet S, Hindle F, Mouret G, Rohart F, Buldyreva J. Analysis of self-broadened pure rotational and rovibrational lines of methyl chloride at room temperature. J Quant Spectrosc Radiat Transfer 2013;116:87-100.

[23] Bray C, Jacquemart D, Lacome N. Temperature dependence for self- and N_2-broadening coefficients of CH_3Cl. J Quant Spectrosc Radiat Transfer 2013;129:186-92.

[24] Bray C, Jacquemart D, Buldyreva J, Lacome N, Perrin A. N_2-broadening coefficients of methyl chloride at room temperature. J Quant Spectrosc Radiat Transfer 2012;113:1102-12.

[25] Barbouchi Ramchani A, Jacquemart D, Dhib M, Aroui H. Theoretical calculations of self-broadening coefficients for the ν_5 band of methyl chloride at various temperatures. J Quant Spectrosc Radiat Transfer 2014;134:1-8.

[26] Barbouchi Ramchani A, Jacquemart D, Dhib M, Aroui H. N_2-broadening coefficients of methyl chloride: measurements at room temperature and calculations at atmospheric temperatures. J Quant Spectrosc Radiat Transfer 2014;148:186-96.

[27] Dudaryonok AS, Lavrentieva NN, Buldyreva LV. CH_3Cl self-broadening coefficients and their temperature dependence. J Quant Spectrosc Radiat Transfer 2013;130:321-6.

[28] Bouanich JP, Blanquet G, Walrand J. Theoretical O_2- and N_2-Broadening Coefficients of CH_3Cl Spectral Lines. J Mol Spectrosc 1993;161:416-26.

[29] Robert D, Bonamy J. Short range force effects in semi-classical molecular line broadening calculations. J Phys 1979;40:923-43.

[30] Buldyreva J, Lavrentieva N, Starikov VI. Collisional lines broadening and shifting of atmospheric gases. London: World Scientific, Imperial College Press :2010.

[31] Faye M, Bordessoule M, Kanouté B, Brubach JB, Roy P, Manceron L. Improved mid infrared detector for high spectral or spatial resolution and synchrotron radiation use. Rev Sci Inst 2016; 87:063119.

[32] Wartewig S. IR and Raman spectroscopy: fundamental processing. Weinheim: Wiley-VCH :2003.

[33] Mertz L. Transformations in optics. New York: Wiley :1965.

[34] Vander Auwera J, Reymond-Laruinaz S, Boudon V, Doizi D, Manceron L. Line intensity measurements and analysis in the ν_3 band of ruthenium tetroxide. J Quant Spectrosc Radiat Transfer 2018;204:103-11.

[35] Vander Auwera J, Vanfleteren T. Line positions and intensities in the 7400–8600 cm^{-1} region of the ammonia spectrum. J Mol Physics 2018;116:1-10.

[36] Tudorie M , Földes T , Vandaele AC , Vander Auwera J . CO_2 pressure broadening and shift coefficients for the 1-0 band of HCl and DCl. J Quant Spectrosc Radiat Transfer 2012;113:1092-101 .

[37] Daneshvar L , Földes T , Buldyreva J , Vander Auwera J . Infrared absorption by pure CO_2 near 3340 cm^{-1}: measurements and analysis of collisional coefficients and line-mixing effects at subatmospheric pressures. J Quant Spectrosc Radiat Transfer

2014;149:258-74.
[38] Hmida F, Galalou S, KwabiaTchana F, Rotger M, Aroui H. Line-mixing effect in the ν_2 band of CH_3Br. J Quant Spectrosc Radiat Transfer 2017;189:351-60.
[39] Pine AS, Markov VN. Self and foreign-gas-broadened line shapes in the ν_1 band of NH_3. J Mol Spectrosc 2004;228:121-42.
[40] Wlodarczak G, Segard B, Legrand J, Demaison J. The dipole moment of $CH_3{}^{35}Cl$, microwave and submillimeterwave spectrum of methyl chloride. J Mol Spectrosc 1985;111:204-6.
[41] Giraud M, Robert D, Galatry L. Citation sur la détermination du moment quadrupolaire de molécules linéaires à partir de l'élargissement des raies spectrales. CR Acad Sci Paris :1971.
[42] Pourcin J, Jacquemoz A, Fournel A, Sielmann H. Pressure broadening of HCl pure rotational lines with a far-infrared optically pumped laser. J Mol Spectrosc 1981;90: 43-50.
[43] Jacquemart D, Kwabia Tchana F, Lacome N, Kleiner I. A complete set of line parameters for CH_3Br in the 10-μm spectral region. J Quant Spectrosc Radiat Transfer 2007;105:264–302.
[44] Jacquemart D, Guinet M. Line parameters measurements and modeling for the ν_6 band of CH_3F: generation of a complete line list for atmospheric databases. J Quant Spectrosc Radiat Transfer 2016;185:58-69.
[45] Buldyreva J, Bonamy J, Robert D. Semi-classical calculations with exact trajectory for N_2 rovibrational Raman linewidths at temperatures below 300 K. J Quant Spectrosc Radiat Transfer 1999;62:321-43.
[46] Buldyreva J, Benec'h S, Chrysos M. Infrared nitrogen-perturbed NO linewidths in a temperature range of atmospheric interest: An extension of the exact trajectory model. Phys Rev 2000;63:012708.
[47] Buldyreva J, Nguyen L. Extension of the exact trajectory model to the case of asymmetric tops and its application to infrared nitrogen-broadened linewidths of ethylene. Phys Rev 2008;77:042720.
[48] Jellali C, Galalou S, Cuisset A, Dhib M, Aroui H. Semi-classical calculations of self-broadening coefficients of OCS and HCN at temperatures between 200 K and 298 K. J Mol Spectrosc 2016;329:35-42.
[49] Starikov VI. Bi-Resonance Functions in the Theory of Collisional Broadening of the Spectral Lines of Molecules. Opt Spectrosc 2012; 112: 27-36.
[50] Leavitt RP. Pressure broadening and shifting in microwave and infrared spectra of molecules of arbitrary symmetry: an irreducible tensor approach. J Chem Phys 1980;73:5432-50.
[51] Gray CG, Gubbins KE. Theory of Molecular Fluids. Oxford University Press, London/New York, 1984.
[52] Birnbaum G. Microwave pressure broadening and its application to intermolecular forces. Adv Chem Phys 1967;12:487-548.